

## Radial x-ray diffraction of tungsten tetraboride to 86 GPa under nonhydrostatic compression

Lun Xiong,<sup>1</sup> Jing Liu,<sup>1,a)</sup> Ligang Bai,<sup>1</sup> Yanchun Li,<sup>1</sup> Chuanlong Lin,<sup>1</sup> Duanwei He,<sup>1</sup> Fang Peng,<sup>2</sup> and Jung-Fu Lin<sup>3</sup>

<sup>1</sup>Beijing Synchrotron Radiation Facility, Institute of High Energy Physics, Chinese Academy of Sciences, Beijing 100049, People's Republic of China

<sup>2</sup>Institute of Atomic and Molecular Physics, Sichun University, Chengdu 610065, People's Republic of China

<sup>3</sup>Department of Geological Sciences, Jackson School of Geosciences, The University of Texas at Austin, Texas 78712, USA

(Received 15 November 2012; accepted 18 December 2012; published online 16 January 2013)

Investigations of the equation of state of tungsten tetraboride (WB<sub>4</sub>) have been performed under nonhydrostatic compression to 85.8 GPa using radial x-ray diffraction techniques in a diamond anvil cell at room temperature. The hexagonal structure of WB<sub>4</sub> is found to be stable up to the highest pressure of 85.8 GPa. The radial x-ray diffraction data yield a bulk modulus  $K_0 = 319(5)$  GPa with  $K'_0 = 4.1(0.2)$  at  $\psi = 54.7^\circ$ . With a fixed  $K'_0$  of 4, the derived  $K_0$  is 323(1) GPa. The bulk modulus obtained from fits of diffraction data at  $\psi = 0^\circ$  and  $90^\circ$  is 196(6) GPa and 507(13) GPa, respectively. The values gradually increased from  $\psi = 0^\circ$  to  $90^\circ$ , showing the compressibility of the sample strongly depends on the stress environment. In addition, the compressibility of the unit cell axes (*a*- and *c*-axes) of WB<sub>4</sub> demonstrates an almost isotropic nature with pressure increasing.

© 2013 American Institute of Physics. [<http://dx.doi.org/10.1063/1.4775482>]

### I. INTRODUCTION

Superhard materials (Vickers hardness  $H_V \geq 40$  GPa) have many superior properties such as the high compressional strength, chemical inertness, and thermal conductivity. One of the outstanding characteristics of superhard materials is their incompressibility.<sup>1</sup> Thus, great efforts involving theoretical and experimental studies in the past few decades have been universally focused on the possibility of establishing new low-compressible materials with bulk moduli and hardness exceeding or closing that of diamond. Tungsten tetraboride (WB<sub>4</sub>) is a candidate superhard materials belonging to the promising groups of transition metal borides. Recently, some experimental and theoretical studies on tungsten tetraboride suggested that WB<sub>4</sub> is a superhard material with a high Vickers hardness (>40 GPa) and a large bulk modulus (~300 GPa).<sup>2-6</sup> In the experimental studies on compressibility, the previous results present some discrepancies of equation of state (EOS) parameters and large relative errors. Gu *et al.*<sup>3</sup> derived the zero-pressure bulk modulus  $K_0 = 200(40)$  GPa with its pressure derivative  $K'_0 = 15.3(5.7)$  from high pressure x-ray diffraction (XRD) data up to 23 GPa with a mixture of methanol, ethanol, and water as the pressure transmission medium. Liu *et al.*<sup>4</sup> performed the high pressure XRD up to 50.8 GPa with silicone oil as medium and obtained  $K_0 = 325(9)$  GPa and  $K'_0 = 5.1 \pm 0.6$ . Mohammadi *et al.*<sup>5</sup> reported a zero-pressure bulk modulus  $K_0$  of 339(3) GPa from high-pressure x-ray diffraction in a Diacell diamond anvil cell with neon gas as the pressure medium up to 30 GPa using the finite strain equation of state ( $K'_0 = 4$ ). More recently, Xie *et al.*<sup>6</sup> measured the compressional behavior of WB<sub>4</sub> with neon gas as the pressure medium up to 58.7 GPa

and obtained a bulk modulus  $K_0 = 326(3)$  with  $K'_0 = 4$  (fixed) and  $K_0 = 369(9)$  with  $K'_0 = 1.2(0.5)$  fitting the data at pressures lower than 42 GPa. The highest pressure in their experiments was 58.4 GPa.<sup>3-6</sup> These results indicate that the pressure transmitting medium plays an important role in the compressibility measurements. Moreover, changing the pressure range can have a significant effect in determination of EOS parameters.

The determination of equation of state greatly depends on the existence of nonhydrostatic stress, especially for superhard materials.<sup>7</sup> However, a completely hydrostatic environment cannot be maintained above 15 GPa due to the freezing of all pressure medium at room temperature.<sup>8-11</sup> Radial x-ray diffraction (RXD) techniques in a DAC together with the lattice strain theory<sup>12-18</sup> can be used to determine the EOS of materials and have been applied to materials such as Au, Re, Mo, tungsten, cubic BC<sub>2</sub>N, etc.<sup>7,19-21</sup> The advantage of RXD is that the EoS can be deduced from the inversion of highly nonhydrostatic compression data without any pressure medium, thus overcoming the limit of pressure transmission medium freezing at very high pressures. Therefore, we have undertaken an experimental study of the pressure-dependent compression behavior of WB<sub>4</sub> using synchrotron angle-dispersive radial x-ray diffraction in a diamond anvil cell to examine the bulk moduli and lattice distortions of WB<sub>4</sub> under pressures by comparison with quasi-hydrostatic results obtained in the conventional diffraction geometry.

In this study, we present the behavior of synthesized tungsten tetraboride in a 2-fold paranomic diamond anvil cell under nonhydrostatic compression up to 85.8 GPa. Using radial x-ray diffraction technique together with the lattice strain theory<sup>12-18</sup> enables us to constrain the compression curve of WB<sub>4</sub> under nonhydrostatic compression to 85.8 GPa.

<sup>a)</sup>Author to whom correspondence should be addressed. Electronic mail: liuj@ihep.ac.cn.

## II. EXPERIMENT

Single-phase  $WB_4$  was synthesized by the hot-pressed method starting with a mixture of W and B, and the synthesized  $WB_4$  has a hexagonal structure (space group  $P6_3/mmc$ ) with lattice parameters  $a = 5.199(0.001)$  Å and  $c = 6.347(0.001)$  Å according to powder x-ray diffraction at ambient conditions. A 2-fold paranomic DAC with a pair of beveled diamond anvils ( $150\ \mu\text{m}$  culet) was used in the RXD measurements. A beryllium gasket was preindented to  $\sim 25\ \mu\text{m}$  thickness and drilled a hole of  $50\ \mu\text{m}$  diameter in the center of preindentation as sample chamber.  $WB_4$  powder was loaded into the gasket hole and a Mo flake with diameter of  $\sim 20\ \mu\text{m}$  was placed on top of the sample serving as a pressure standard<sup>23</sup> as well as the sample position reference. No pressure-transmitting medium was used to ensure maximum nonhydrostatic stresses. The angle-dispersive radial x-ray diffraction experiments were performed on 4W2 beamline at the Beijing Synchrotron Radiation Facility (BSRF), Chinese Academy of Sciences. A Si(111) monochromator was used to tune the synchrotron source with a wavelength of  $0.6199$  Å, and the incident monochromatic x-ray beam was focused to a  $26 \times 8\ \mu\text{m}^2$  full width at half maximum (FWHM) spot by a pair of Kirkpatrick-Baez mirrors. Two-dimensional diffraction patterns were collected by a Mar345 image plate detector and analyzed with the program Fit2D.<sup>24</sup> The distance and orientation of the detector were calibrated using a  $CeO_2$  standard. At each increasing pressure, the RXD pattern was collected after about 30 min to allow for stress relaxation.

In a normal angle-dispersive radial x-ray diffraction experiment, the incident x-ray is perpendicular to the compression axis and passes through a Be gasket. In order to minimize the contribution of Be diffraction lines to the sample patterns, the DAC was tilted to a  $\alpha$  angle of  $28^\circ$  (see Fig. 1).<sup>14</sup> In this geometry, the  $\psi$  corresponding to the angle between the diffracting plane normal and the loading axis was calculated using the equation<sup>22</sup>

$$\cos \psi_{hkl} = \sin \alpha \cos \delta \cos \theta_{hkl} + \cos \alpha \sin \theta_{hkl}, \quad (1)$$

where  $\theta$  is the diffraction angle and  $\delta$  is the azimuthal angle in the plane of the detector.

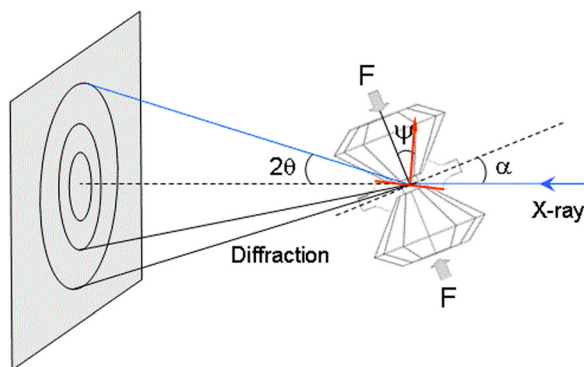


FIG. 1. Radial x-ray diffraction geometry used with a diamond anvil cell. The DAC was tilted to an  $\alpha$  angle of  $28^\circ$ .

## III. THEORY

According to the lattice strain theory,<sup>12–18</sup> the stress state at the center of the compressed polycrystalline sample under uniaxial loading in a diamond anvil cell is characterized by  $\sigma_1$  and  $\sigma_3$ , which is the maximum stress along the DAC loading axis and the minimum stress in the radial direction, respectively.  $\sigma_P$  is the mean normal stress and is equal to  $(2\sigma_3 + \sigma_1)/3$ . The difference between  $\sigma_3$  and  $\sigma_1$  is the macroscopic differential stress,  $t$  ( $t = \sigma_3 - \sigma_1$ ).

The measured  $d$ -spacing  $d_m(hkl)$  is a function of the azimuthal angle  $\psi$  between the diamond cell loading axis and the diffraction plane normal and diffraction plane ( $hkl$ )

$$d_m(hkl) = d_p(hkl)[1 + (1 - 3 \cos^2 \psi)Q(hkl)], \quad (2)$$

where  $d_m(hkl)$  is the measured  $d$  spacing,  $d_p(hkl)$  is the  $d$  spacing due to the hydrostatic component of stress, and  $Q(hkl)$  is the orientation dependent lattice strain.<sup>14–17</sup>

Eq. (2) suggests that  $d_m(hkl)$  should vary linearly with  $1 - 3 \cos^2 \psi$ , reaching a maximum at  $\psi = 90^\circ$  and minimum at  $\psi = 0^\circ$ , respectively. At  $\psi = 54.7^\circ$  ( $1 - 3 \cos^2 \psi = 0$ ), the position of the observed x-ray diffraction lines reflects the  $d$  spacing due to the mean component of stress, so the equivalent hydrostatic compression curve can be directly derived from the diffraction data at  $\psi = 54.7^\circ$ . The slope of the  $d_m(hkl)$  versus  $1 - 3 \cos^2 \psi$  relation yields the product  $d_p(hkl)Q(hkl)$  and  $d_p(hkl)$  can be directly measured at  $\psi = 54.7^\circ$ .

## IV. RESULTS AND DISCUSSION

The RXD diffraction patterns are integrated over each azimuthal sectors with  $5^\circ$  interval using Fit2D<sup>24</sup> for data analyses. The program Multifit 4.2 is used to perform macro decomposition of 2D diffraction images into azimuthal slices using Fit2D<sup>24</sup> to yield one-dimensional plots of x-ray intensity as a function of two-theta and fits peak positions, intensities, and FWHM of the diffraction peaks. To determine the variation of the diffraction peaks' positions with  $\delta$ , we used this software package to integrate the diffraction patterns and fit peak positions with segments of  $5^\circ$  intervals in the azimuth angle, in steps from  $180^\circ$  to  $270^\circ$ . Radial x-ray diffraction spectra of  $WB_4$  were collected up to an equivalent pressure of  $85.8$  GPa, where pressures were derived from the equation of state of Mo<sup>23</sup> using the unit cell volume obtained from the  $d_p(110)$  of Mo at  $\psi = 54.7^\circ$ .

Fig. 2 shows the selected diffraction patterns of the sample taken at  $\psi_{hkl} = 54.7^\circ$  under different pressures. Diffraction peak positions were fitted with Pseudo-Voigt line shapes using the software package Multifit 4.2. Though seven diffraction peaks of  $WB_4$  (101, 002, 110, 201, 112, 103, 211) were observed in most diffraction patterns, the (002, 201, 103, 211) peaks were relatively weaker, whereas the (110) peak begins to split at  $45.0$  GPa. One of the possible reasons for the splitting of  $WB_4$  (110) diffraction line is that the grain size of  $WB_4$  is not homogeneous ( $0.5\ \mu\text{m}$ – $1.5\ \mu\text{m}$ ) and some bigger grains in a nonhydrostatic stress result in the discontinuity of pressure then the split of peak. The bigger grains near the edge of the sample chamber likely suffered lower pressure as to generate the peak with lower  $2\theta$  angle, as

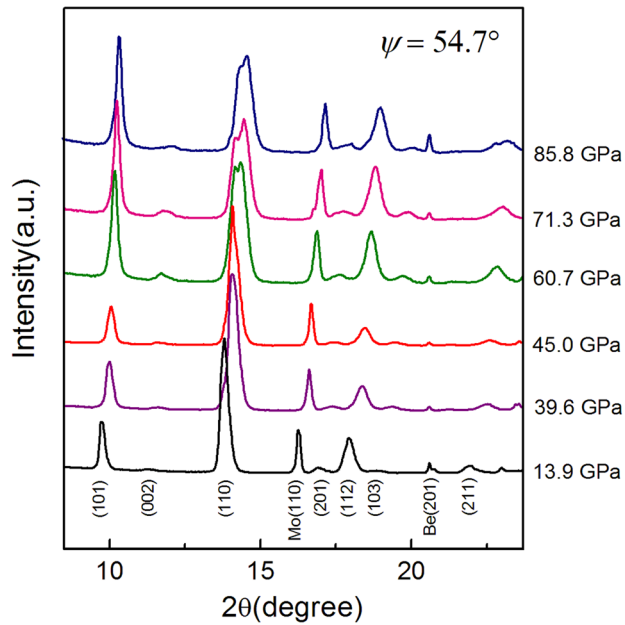


FIG. 2. Selected diffraction patterns of  $WB_4$  under nonhydrostatic compression taken at  $\psi = 54.7^\circ$ . The pressures are determined from the Mo(110) at  $\psi = 54.7^\circ$ . The estimated errors are obtained from the scatter of  $d(hkl)$  versus  $1-3\cos^2\psi$ .

shown in Fig. 2. Another reason for the peak splitting may be that the strong shear stress under uniaxial compression causes to a change in the crystal structure. But this needs further examination.

The  $d_m(hkl)$  variation with  $1-3\cos^2\psi$  for  $WB_4$  (101), (110), (112), and (201) diffraction lines at six selected pressures is shown in Fig. 3. The  $d$ -spacing of the  $WB_4$  (110) diffraction line is obtained from a stronger peak position after 45.0 GPa. As expected from the theory, the measured  $d$ -spacings vary linearly with  $1-3\cos^2\psi$ .

The  $d$ -spacings of  $d_p(101)$ ,  $d_p(201)$ ,  $d_p(112)$  and  $d_p(211)$ , corresponding to hydrostatic components of stress, were derived from the intercept of the  $d_m(hkl)$  versus  $1-3\cos^2\psi$  relation at  $(1-3\cos^2\psi)=0$  ( $\psi=54.7^\circ$ ) and used to calculate the lattice parameters fitting to a hexagonal cell. The normalized unit cell volume of compression curves for  $\psi = 0^\circ$ ,  $\psi = 54.7^\circ$ , and  $\psi = 90^\circ$  are shown in Fig. 4. For comparison, the results obtained in earlier normal XRD under quasi-hydrostatic compression were also included.<sup>3,4,6</sup> Angles  $\psi = 0^\circ$  and  $90^\circ$  represent the diffracting plane normal being parallel and perpendicular to the load axis respectively, and the stress environment of the sample is maximum and minimum respectively. It is evident from Fig. 4 that our experimental data have very good fitting precision.

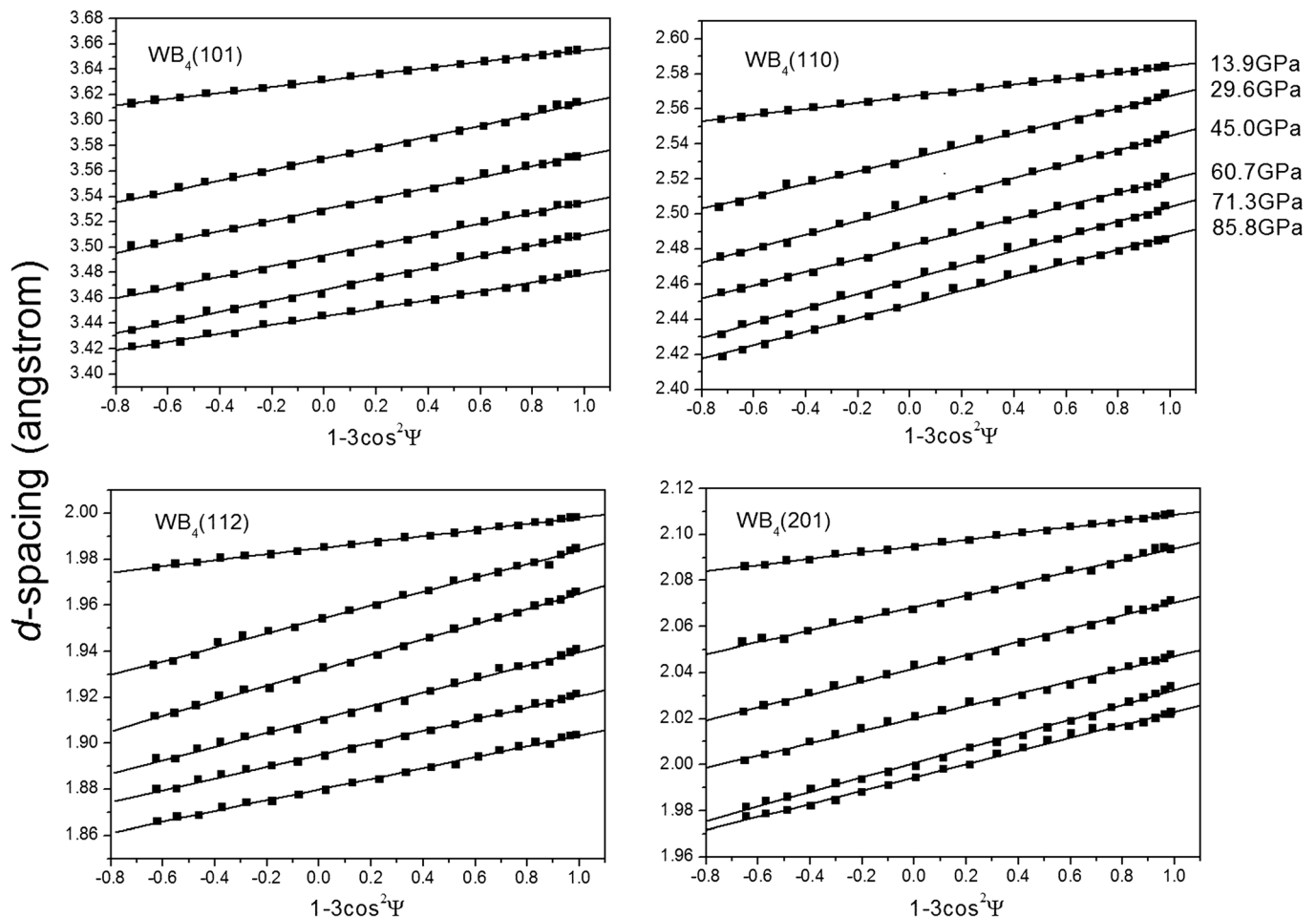


FIG. 3. Dependence of observed  $d$ -spacing on  $1-3\cos^2\psi$  for the  $WB_4$  (101), (110), (112), and (201) diffraction lines at different pressures. The solid lines are least-squares fits to the data.

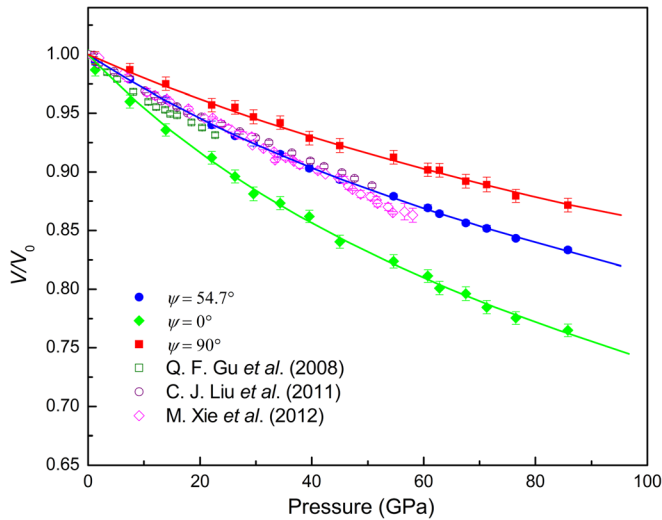


FIG. 4. Compression curves of  $\text{WB}_4$  from lattice parameters measured at  $0^\circ$ ,  $54.7^\circ$ , and  $90^\circ$ . The solid lines are Birch-Murnaghan equation fitting lines to the data at each angle. Other reported compression data of  $\text{WB}_4$  are also shown for comparison. The open circles are the static compression data of Ref. 3. The open squares are the static compression data obtained by Liu *et al.* of Ref. 4. The open diamonds are the static compression data of Ref. 6.

The unit cell volumes as a function of pressure were fitted using third-order Birch–Murnaghan EOS to obtain the ambient pressure bulk modulus  $K_0$  and its pressure derivative  $K'_0$ . The third-order Birch–Murnaghan EOS is expressed as follows:<sup>25</sup>

$$P = 1.5K_0 \left[ \left( \frac{V_0}{V} \right)^{\frac{2}{3}} - \left( \frac{V_0}{V} \right)^{\frac{5}{3}} \right] \left\{ 1 + \frac{3}{4}(K'_0 - 4) \left[ \left( \frac{V_0}{V} \right)^{\frac{2}{3}} - 1 \right] \right\}, \quad (3)$$

where  $K_0$ ,  $K'_0$ , and  $V_0$  are the bulk modulus, its pressure derivative, and the unit-cell volume at ambient conditions, respectively. Through fitting the diffraction data at  $\psi = 54.7^\circ$  up to 86 GPa by Eq. (3), we obtain the bulk module  $K_0 = 319(5)$  GPa and its pressure derivative  $K'_0 = 4.1(0.2)$ .

With a fixed  $K'_0$  of 4, the least-squares fit yields an ambient bulk modulus the derived  $K_0 = 323(1)$  GPa. The bulk modulus obtained from fits of diffraction data at  $\psi = 0^\circ$  and  $90^\circ$  is 196(6) GPa and 507(13) GPa, respectively. Angles  $\psi = 0^\circ$  and  $90^\circ$  represent the diffracting plane normal being parallel and perpendicular to the load axis respectively, and the stress environment of the sample is maximum and minimum, respectively.

A comparison between our research results and the previously reported data<sup>2–6</sup> on the bulk modulus ( $K_0$ ) and its pressure derivative ( $K'_0$ ) is shown in Table I. It can be seen that, the comparison of the bulk modulus derived from different  $\psi$  suggests a variation of a factor of 2.6 between  $\psi = 0^\circ$  and  $\psi = 90^\circ$ . The values gradually increased from  $\psi = 0^\circ$  to  $\psi = 90^\circ$ , showing the compressibility of the sample strongly depends on the stress environment. In addition, the bulk modulus of  $\text{WB}_4$  obtained here under uniaxial compression at  $\psi = 54.7^\circ$  is in roughly consistent with that from x-ray diffraction under quasi-hydrostatic condition obtained from Xie *et al.* within the experimental error as well as in accord with the value obtained by theoretical calculation

TABLE I. A summary of the bulk modulus ( $K_0$ ) of  $\text{WB}_4$  and their pressure derivative ( $K'_0$ ) obtained from various methods. Asterisk indicates methanol-ethanol mixture in the volume ratio of 4:1. GGA refers to the generalized gradient approximation; LDA refers to local density approximation; PTM refers to pressure-transmitting medium.

$K_0$ (GPa)	$K'_0$	$P_{max}$ (GPa)	Method and PTM	Reference
323(1)	4(fixed)	85.8	RXD ( $\psi = 54.7^\circ$ ), null	This work
319(5)	4.1(0.2)		RXD ( $\psi = 54.7^\circ$ ), null	
196(6)	3.6(0.2)		RXD ( $\psi = 0^\circ$ ), null	
507(13)	2.9(0.4)		RXD ( $\psi = 90^\circ$ ), null	
200(40)	15.3(5.7)	23	XRD, alcohol*	Gu <i>et al.</i> <sup>3</sup>
304(10)	4(fixed)			
325(9)	5.1(6)	50.8	XRD, silicone oil	Liu <i>et al.</i> <sup>4</sup>
342(3)	4(fixed)			
339(3)	4(fixed)	30	XRD, neon gas	Mohammadi <i>et al.</i> <sup>5</sup>
326(3)	4(fixed)	42	XRD, neon gas	Xie <i>et al.</i> <sup>6</sup>
369(9)	1.2(0.5)			
292.7			Theory (GGA)	Wang <i>et al.</i> <sup>2</sup>
324.3			Theory (LDA)	

local density approximation (LDA),<sup>2–6</sup> while it is much bigger than 200(40) GPa obtained by Gu *et al.*<sup>3</sup> The pressure derivative obtained from third-order Birch-Murnaghan equation of state is very close to 4 and the values of  $K_0$  are in highly consistent, demonstrating that we obtained good results for hydrostatic condition. Due to the freezing of all known pressure media at high pressures, a completely hydrostatic environment cannot be retained above 15 GPa.<sup>8–11</sup> This has an effect of overestimating the equation of state parameters. As a consequence, using radial x-ray diffraction techniques in a pressure cell can have the profound advantages when investigating the equations of state of superhard materials such as  $\text{WB}_4$  at very high pressures.

The pressure dependence of the normalized lattice parameters of the hexagonal phase compared with the results reported previously.<sup>3,4,6</sup> is shown in Fig. 5. The fitting result of entire pressure range yields

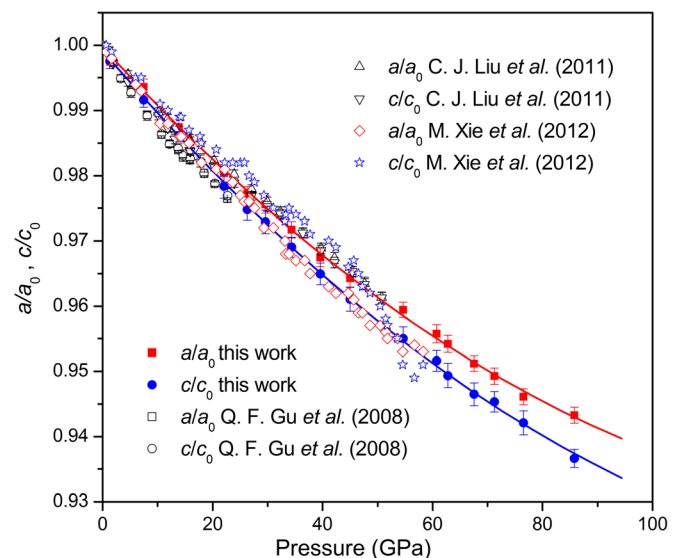


FIG. 5. Compressibility of the normalized lattice parameters of  $\text{WB}_4$  compared with the data obtained by Gu *et al.* (Ref. 3), Liu *et al.* (Ref. 4), and Xie *et al.* (Ref. 6).

$$\frac{a}{a_0} = 1 - 9.2 \times 10^{-4} \left( \frac{P}{P_0} \right) + 3.0 \times 10^{-6} \left( \frac{P}{P_0} \right)^2 \quad (4)$$

and

$$\frac{c}{c_0} = 1 - 9.8 \times 10^{-4} \left( \frac{P}{P_0} \right) + 3.0 \times 10^{-6} \left( \frac{P}{P_0} \right)^2. \quad (5)$$

The relative change along the *a*-axis is about 5.5% and that along the *c*-axis is about 6.1% from 1.4 GPa to 85.8 GPa. The axial compression is almost isotropic as both axes have a similar compressibility, which is in good agreement with Gu *et al.* and Xie *et al.*'s conclusion.<sup>3,6</sup> The reason for its isotropic nature of compressibility different from usual hexagonal structure materials is that the unique covalent bonding network, with B-B covalent bonds aligned along the *c*-axis results in a quasi-isotropic compressibility.<sup>3,6</sup>

The compression behavior of the *a*- and *c*-axes shows a good regularity in the entire pressure range investigated in contrast to that derived from the measurements by Liu *et al.* and Xie *et al.*<sup>4,6</sup> At higher pressures, after about 25 GPa reported by Liu *et al.*,<sup>4</sup> the compression behavior of the *a*- and *c*-axes is likely to be abnormal. The authors interpreted the freezing of silicone oil at high pressures and the increasing of the uniaxial stress component.<sup>8,10,11</sup> Xie *et al.* reported that the *c* axis suddenly undergoes a softening and becomes significantly more compressible than the *a*-axis at ~42 GPa, while, *a*-axis does not show any change in behavior. Due to the WB<sub>4</sub> diffraction patterns remaining the same, with no observation of peak broadening or splitting at the point of the structural change at 42 GPa, and the *c*-lattice constant recovering its original strain values upon decompression, they assigned that anomaly to a structurally induced reversible second-order phase transition because of the three-dimensional, almost isotropic, rigid covalently boron network.<sup>6</sup> The *c*-axes uncompressibility obtained from Xie *et al.* is a little higher than the *a*-axes uncompressibility, whereas our research results and the results obtained from Liu *et al.* show an oppose conclusion.<sup>4,6</sup> The differences may be due to different synthesizing methods, grain sizes of different starting materials, and/or hydrostaticity.

## V. CONCLUSION

Using radial x-ray diffraction technique together with the lattice strain theory, we examined the behavior of WB<sub>4</sub> in a diamond anvil cell under nonhydrostatic compression up to 85.8 GPa. The bulk modulus of WB<sub>4</sub> derived from the nonhydrostatic compression data can vary nearly a factor of 2.6 depending on the relative orientation of the diffraction normal and diamond cell stress axis. The compression curve obtained at  $\psi = 54.7^\circ$  yields a bulk modulus  $K_0 = 319(5)$  GPa and its pressure derivative  $K'_0 = 4.1(0.2)$ . The bulk modulus under  $\psi = 54.7^\circ$  is close to previous experimental results under quasi-hydrostatic conditions derived from Xie *et al.* and the theoretically predicted value. In addition, the

compressibility of the unit cell axes (*a*- and *c*-axes) of WB<sub>4</sub> demonstrates an almost isotropic nature and a good regularity with pressure increasing.

## ACKNOWLEDGMENTS

The authors thank Xiaodong Li and Haini Dong for technical assistance and helpful discussion. Financial supports from the National Natural Science Foundation of China (Nos.10875142 and 11079040, 11027405, and 10976018) and the National Basic Research Program of China (No. 2011CB808200) are gratefully acknowledged. This work was performed at 4W2 beamline of Beijing Synchrotron Radiation Facility (BSRF), which is supported by Chinese Academy of Sciences under Grant Nos. KJCX2-SWN03 and KJCX2-SW-N20. J.F.L acknowledges support from Energy Frontier Research in Extreme Environments (EFree) and the Carnegie/DOE Alliance Center (CDAC).

- <sup>1</sup>C. M. Sung and M. Sung, *Mater. Chem. Phys.* **43**, 1 (1996).
- <sup>2</sup>M. Wang, Y. W. Li, T. Cui, Y. M. Ma, and G. T. Zou, *Appl. Phys. Lett.* **93**, 101905 (2008).
- <sup>3</sup>Q. F. Gu, G. Krauss, and W. Steurer, *Adv. Mater.* **20**, 3620 (2008).
- <sup>4</sup>C. J. Liu, F. Peng, N. Tan, J. Liu, F. J. Li, J. Q. Qin, J. H. Wang, Q. M. Wang, and D. W. He, *High Press. Res.* **31**, 275 (2011).
- <sup>5</sup>R. Mohammadi, A. T. Lech, M. Xie, B. E. Weaver, M. T. Yeung, S. H. Tolbert, and R. B. Kaner, *Proc. Natl. Acad. Sci. U.S.A.* **108**, 10958 (2011).
- <sup>6</sup>M. Xie, R. Mohammadi, Z. Mao, M. M. Armentrout, A. Kavner, R. B. Kaner, and S. H. Tolbert, *Phys. Rev. B* **85**, 064118 (2012).
- <sup>7</sup>D. W. He and T. S. Duffy, *Phys. Rev. B* **73**, 134106 (2006).
- <sup>8</sup>I. Fujishiro, G. J. Piermarini, S. Block, and R. G. Munro, "High pressure in research and industry," in *Proceedings of the 8th AIRAPT Conference Uppsala*, edited by C. M. Backman, T. Johannisson, and L. Tegner (ISBN, Sweden, 1982), Vol. II, p. 608.
- <sup>9</sup>P. M. Bell and H. K. Mao, *Annual Report, year book of the Carnegie Institution*, (G. P. O., Washington, D. C., 1975), p. 399.
- <sup>10</sup>D. D. Ragan, D. R. Clarke, and D. Schiferl, *Rev. Sci. Instrum.* **67**, 494 (1996).
- <sup>11</sup>Y. R. Shen, R. S. Kumar, M. Pravica, and M. F. Nicol, *Rev. Sci. Instrum.* **75**, 4450 (2004).
- <sup>12</sup>A. K. Singh, *J. Appl. Phys.* **73**, 4278 (1993).
- <sup>13</sup>A. K. Singh, C. Balasingh, H. K. Mao, R. J. Hemley, and J. F. Shu, *J. Appl. Phys.* **83**, 7567 (1998).
- <sup>14</sup>A. K. Singh, *J. Phys. Chem. Solids* **65**, 1589 (2004).
- <sup>15</sup>A. K. Singh and C. Balasingh, *J. Appl. Phys.* **75**, 4956 (1994).
- <sup>16</sup>A. K. Singh, H. K. Mao, J. F. Shu, and R. J. Hemley, *Phys. Rev. Lett.* **80**, 2157 (1998).
- <sup>17</sup>A. K. Singh, *J. Appl. Phys.* **106**, 043514 (2009).
- <sup>18</sup>A. K. Singh and H. P. Liermann, *J. Appl. Phys.* **109**, 113539 (2011).
- <sup>19</sup>H. N. Dong, D. W. He, T. S. Duffy, and Y. S. Zhao, *Phys. Rev. B* **79**, 014105 (2009).
- <sup>20</sup>T. S. Duffy, G. Y. Shen, J. F. Shu, H. K. Mao, R. J. Hemley, and A. K. Singh, *J. Appl. Phys.* **86**, 6729 (1999).
- <sup>21</sup>T. S. Duffy, G. Y. Shen, D. L. Heinz, J. F. Shu, Y. Z. Ma, H. K. Mao, R. J. Hemley, and A. K. Singh, *Phys. Rev. B* **60**, 15063 (1999).
- <sup>22</sup>S. Merkel, H. R. Wenk, J. F. Shu, G. Y. Shen, P. Gillet, H. K. Mao, and R. J. Hemley, *J. Geophys. Res.* **107**, 2271, doi:10.1029/2001JB000920 (2002).
- <sup>23</sup>R. S. Hixson and J. N. Fritz, *J. Appl. Phys.* **71**, 1721 (1992).
- <sup>24</sup>A. P. Hammersley, S. O. Svensson, M. Hanfland, A. N. Fitch, and D. Häusermann, *High Press. Res.* **14**, 235 (1996).
- <sup>25</sup>F. Birch, *J. Geophys. Res.* **83**, 1257, doi:10.1029/JB083iB03p01257 (1978).